A developmentally regulated Na-H exchanger in *Dictyostelium discoideum* is necessary for cell polarity during chemotaxis

Hitesh Patel and Diane L. Barber

Department of Cell and Tissue Biology, University of California, San Francisco, San Francisco, CA 94143

Increased intracellular H^+ efflux is speculated to be an evolutionarily conserved mechanism necessary for rapid assembly of cytoskeletal filaments and for morphological polarity during cell motility. In *Dictyostelium discoideum*, increased intracellular pH through undefined transport mechanisms plays a key role in directed cell movement. We report that a developmentally regulated Na-H exchanger in *Dictyostelium discoideum* (*Dd*NHE1) localizes to the leading edge of polarized cells and is necessary for intracellular pH homeostasis and for efficient chemotaxis. Starved *Dd*NHE1-null cells (*Ddnhe1*$^-$) differentiate, and in response to the chemoattractant cAMP they retain directional sensing; however, they cannot attain a polarized morphology, but instead extend mislocalized pseudopodia around the cell and exhibit decreased velocity. Consistent with impaired polarity, in response to chemoattractant, *Ddnhe1*$^-$ cells lack a leading edge localization of F-actin and have significantly attenuated de novo F-actin polymerization but increased abundance of membrane-associated phosphatidylinositol 3,4,5-trisphosphate ($PI_{(3,4,5)}P_3$). These findings indicate that during chemotaxis *Dd*NHE1 is necessary for establishing the kinetics of actin polymerization and $PI_{(3,4,5)}P_3$ production and for attaining a polarized phenotype.

Introduction

The slime mold *Dictyostelium discoideum* has been extensively studied as a model for eukaryotic chemotaxis because many of the molecules and principles that underlie chemotaxis are common to both *Dictyostelium* and mammalian cells (Parent, 2004). Chemotactic competence of *Dictyostelium* cells toward cAMP can be efficiently and synchronously induced by starvation of vegetative cells. Chemotactically competent cells adopt a classical polarized, elongated morphology while chemotaxing and have a defined front, which is more sensitive to cAMP than the cell rear.

Efficient chemotaxis entails two distinct but functionally linked components: directional sensing and polarity (Devreotes and Janetopoulos, 2003). Directional sensing, defined as the ability of a cell to perceive a signal and set up an initial internal asymmetry in the direction of the incoming signal, requires an asymmetric production of the lipid second messenger phosphatidylinositol 3,4,5-trisphosphate ($PI_{(3,4,5)}P_3$) but is independent of actin polymerization. Polarity reinforces internal asymmetries and translates them into relevant morphological changes to execute efficient movement toward chemoattractants. In contrast to directional sensing, localized actin polymerization, regulated predominantly by the localized activation of Rho family low molecular weight GTPases, is a conserved core determinant in cell polarity from yeasts to mammalian cells (Etienne-Manneville and Hall, 2002; Nelson, 2003). In chemotaxing neutrophils, actin polymerization at the leading edge of the cell acts in a positive feedback loop to reinforce localized production of $PI_{(3,4,5)}P_3$ and activation of the Rho family GTPase Rac (Weiner et al., 2002; Srinivasan et al., 2003), and in motile cells, including chemotaxing *Dictyostelium* cells, de novo actin polymerization is a predominant driving force for membrane protrusions or pseudopodia (Condeelis et al., 1990; Pollard and Borisy, 2003).

A long-speculated but poorly understood mechanism promoting de novo actin polymerization during cell movement is an increase in intracellular pH (pH_i). Earlier work on the fertilization of sea urchin eggs (Begg and Rebhun, 1979) and the acrosomal reaction in Echinoderm sperm cells (Tilney et al., 1978) indicates that transient increases in pH_i are necessary for actin polymerization and that artificially increasing pH_i in the absence of external cues triggers F-actin formation. In *Ascaris* sperm cells, a pH_i gradient that is higher at the front of the cell than at the rear is necessary for cell polarity and a leading

Correspondence to Diane L. Barber: barber@itsa.ucsf.edu

Abbreviations used in this paper: CRAC, cytosolic regulator of adenylyl cyclase; PH, pleckstrin homology; pH_i, intracellular pH; PI3, phosphatidylinositol 3; $PI_{(3,4,5)}P_3$, phosphatidylinositol 3,4,5-trisphosphate.

The Journal of Cell Biology, Vol. 169, No. 2, April 25, 2005 321–329
http://www.jcb.org/cgi/doi/10.1083/jcb.200412145

edge assembly of cytoskeletal filaments (King et al., 1994; Italiano et al., 1999), even though motile *Ascaris* sperm cells lack actin and cytoskeletal filaments consist of bundled fibers of major sperm protein. In mammalian fibroblasts (Denker and Barber, 2002) and sperm cells (Wang et al., 2003), H^+ efflux by plasma membrane isoforms of the Na-H exchanger, NHE, is necessary for directed migration and motility, respectively, although effects of NHE on actin polymerization have not been determined. In *Dictyostelium* cells, increases in pH_i promote chemotaxis (Van Duijn and Inouye, 1991); however, the ion transport mechanisms regulating pH_i homeostasis in *Dictyostelium* have not been clearly defined.

We now report that a *Dictyostelium* Na-H exchanger, *Dd*NHE1, is necessary for cell polarity and chemotaxis in response to cAMP. *Dd*NHE1 is developmentally expressed with chemotactic competence, is predominantly localized at the front of chemotaxing cells, and is necessary for cAMP-induced increases in pH_i. In response to a gradient of cAMP, *Ddnhe1*-null (*Ddnhe1*$^-$) cells are unable to polarize, retain a rounded morphology, and extend pseudopodia around the cell periphery. Although *Ddnhe1*$^-$ cells retain directional sensing of cAMP, chemotaxis is impaired. *Ddnhe1*$^-$ cells lack an asymmetric localization of F-actin at the leading edge, and early and late phases of the biphasic increase in actin polymerization are attenuated compared with wild-type Ax2 cells. Stable expression of *Dd*NHE1 in *Ddnhe1*$^-$ cells restores a polarized morphology, pseudopodia that are restricted to the leading edge, the kinetics of actin polymerization, and efficient chemotaxis. These findings demonstrate that *Dd*NHE1 is necessary for chemotaxing *Dictyostelium* cells to regulate localized actin polymerization and to adopt a polarized phenotype.

Results

*Dd*NHE1 is developmentally expressed and is necessary for pH_i homeostasis but not for cell differentiation

A single Na-H exchanger, *Dd*NHE1 (AAO52201), has been found by the *Dictyostelium* Sequencing Project. By hydropathy plot analysis, *Dd*NHE1 is predicted to contain twelve transmembrane segments and a hydrophilic COOH-terminal domain, which is consistent with NHE isoforms in other species. Sequence alignment with identified NHEs using ClustalW software (www.ebi.ac.uk/clustalw/) groups *Dd*NHE1 with mammalian NHE8 and *Drosophila melanogaster* NHE1 (Fig. 1 A). Mammalian NHE8 groups in a clade distinct from the clade including mammalian NHE1, which is a resident plasma membrane isoform, and from the clade including mammalian NHE6 and NHE7, which are intracellular vesicle isoforms. The mouse orthologue MmNHE8 is a recycling plasma membrane protein and localizes at the apical plasma membrane and at intracellular organelle membranes in kidney proximal tubule cells (Goyal et al., 2003). The localization of *Dd*NHE1 is predicted to be at the plasma membrane with ~74% probability, as determined by the PSORT II localization software (www.psort.org). Immunolabeling of *Dd*NHE1-HA stably expressed in wild-type Ax2 cells indicated a plasma membrane and an intracellular distribution, suggesting it is a recycling plasma membrane isoform, like MmNHE8. In polarized chemotaxing cells, intracellular and plasma membrane *Dd*NHE1-HA localized predominantly at the cell front (Fig. 1 B), and cell surface biotinylation was used to confirm that *Dd*NHE1-HA is at the plasma membrane (Fig. 1 C). Mammalian NHE1 has a similar localization at the leading edge plasma membrane of lamellipodia in migrating fibroblasts (Denker et al., 2000; Denker and Barber, 2002).

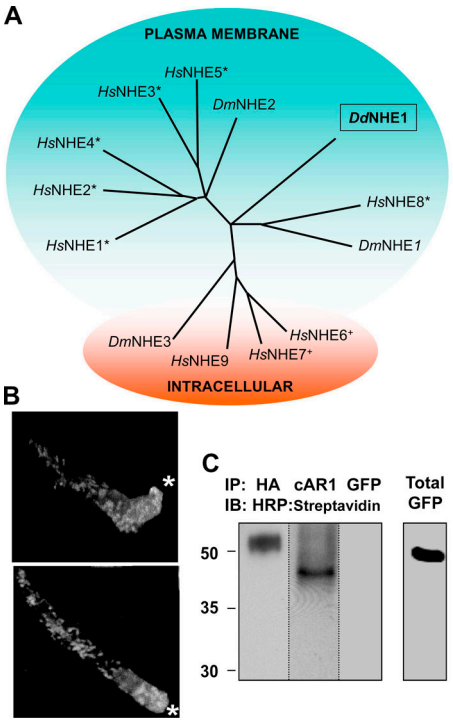

Figure 1. ***Dd*NHE1 groups with plasma membrane NHEs and localizes to the leading edge of chemotaxing cells.** (A) *Dictyostelium* NHE1 (*Dd*NHE1; AA052201), the nine known mammalian NHEs (*Hs*NHE1–9; P19634, Q9UBY0, P48764, XM_371544.2, Q14940, Q92581, Q96T83, Q9Y2E8, and Q8IVB4, respectively), and three *Drosophila* NHEs (*Dm*NHE1–3; Q8SZX8, Q9VIF9, and Q81PJ4, respectively) were aligned using ClustalW; the resulting tree diagram is shown. An asterisk (plasma membrane) or plus (intracellular membranes) denotes NHEs confirmed to have the indicated localization. (B) Localization of *Dd*NHE1-HA in chemotaxing cells, as determined by immunolabeling with anti-HA antibodies, was visualized by confocal microscopy. The three-dimensional projection of two representative cells is shown. White asterisks indicate direction of the point source of cAMP delivered by a micropipette. (C) Surface biotinylation followed by immunoprecipitating the indicated proteins and immunoblotting with HRP:Streptavidin-confirmed *Dd*NHE1-HA is at the plasma membrane. Immunoprecipitation of the plasma membrane cAMP receptor 1 (cAR1) in cells expressing *Dd*NHE1-HA and the GFP-tagged PH domain of CRAC (GFP-PH^{CRAC}) expressed in Ax2 cells were included as positive and negative controls, respectively. Immunoblot of total PH^{CRAC}:GFP is shown separately (right).

The transition of vegetative *Dictyostelium* cells to chemotactically competent cells is induced by starvation and requires the expression of several genes that allow cells to make, sense, break down, and move toward cAMP. In addition to expressing genes required for chemotaxis, starvation induces genes involved in cell differentiation. The *Dd*NHE1 transcript was detected in chemotactically competent cells, but not in vegetative cells (Fig. 2 A), which suggests a role for *Dd*NHE1 in chemotaxis, differentiation, or both processes.

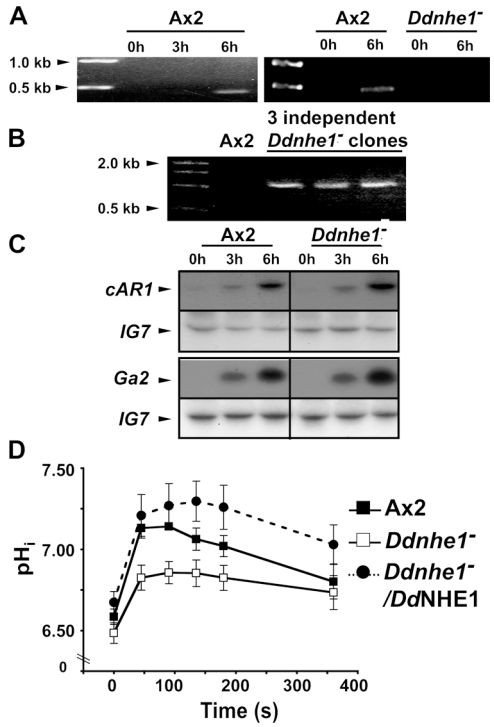

Figure 2. ***Dd*NHE1 expression is developmentally regulated and is necessary for increased pH_i in response to cAMP but is not necessary for developmentally regulated expression of cAR1 and Gα2.** (A) Expression of the *Dd*NHE1 transcript in Ax2 cells is induced after 6 h of starvation (left). *Dd*NHE1 transcript is lost in a representative clone of *Ddnhe1*$^-$ cells (right). (B) *Ddnhe1*$^-$cells identified by the presence of a 1-kb PCR product that is absent from Ax2 cells. Samples from three independently generated *Ddnhe1*$^-$ clones are shown. (C) Expression of *cAR1* and *Gα2* is similar in Ax2 and *Ddnhe1*$^-$ cells, as determined by Northern blot analysis. Expression of the ribosomal gene IG7 was used as a loading control. (D) pH_i in the absence and presence of cAMP in chemotactically competent Ax2 (closed squares), *Ddnhe1*$^-$ (open squares), and *Ddnhe1*$^-$*/Dd*NHE1 (closed circles) cells was determined in cells loaded with the fluorescent pH-sensitive dye BCECF. Data are expressed as the mean ± SEM of three independent experiments.

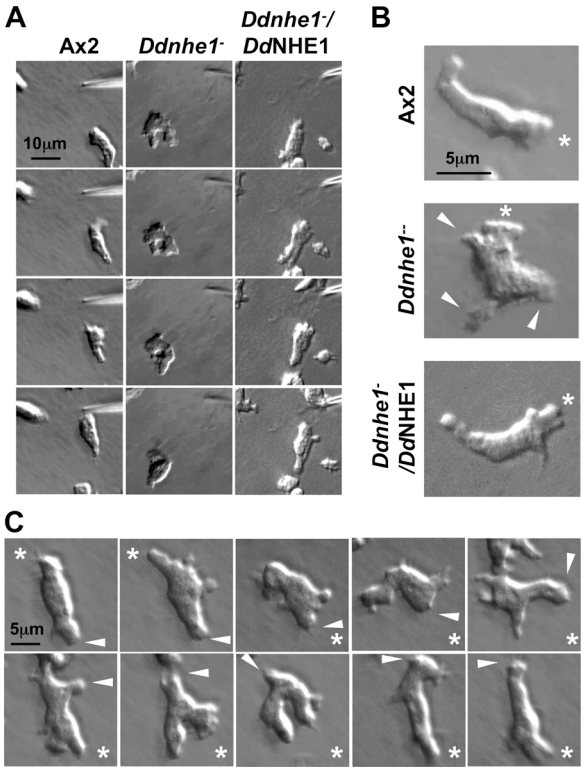

Figure 3. ***Ddnhe1*$^-$ cells are unable to polarize.** (A) In response to a point source of cAMP delivered by a micropipette, Ax2 (left) and *Ddnhe1*$^-$*/Dd*NHE1 (right) cells adopt an elongated, polarized morphology with a clearly defined front as cells move toward the chemoattractant source (Videos 1 and 3). *Ddnhe1*$^-$ cells lack polarity (middle) and, over the time course shown, fail to move toward the chemoattractant source (Video 2). (B) Polarized Ax2 and *Ddnhe1*$^-$*/Dd*NHE1 cells extend pseudopods only from their leading edges (top and bottom), but *Ddnhe1*$^-$ cells remain unpolarized and extend pseudopods around the cell periphery (middle). Asterisks represent the location of the micropipette containing cAMP. Arrowheads indicate extension of pseudopods along the periphery of *Ddnhe1*$^-$ cells. (C) In response to a change in direction of the point source of cAMP, Ax2 cells retain the same leading and trailing edges and execute turns to continue moving toward the chemoattractant. The arrowheads indicate the rear of the cell. Asterisks are the same as in B.

To determine the functional importance of *Dd*NHE1, we generated *Dd*nhe1-null (*Ddnhe1*$^-$) cells. Ax2 cells were transformed by linearized DNA constructs designed to disrupt the *Ddnhe1* gene. Individual clones, each generated by using a different construct to disrupt *Ddnhe1,* were selected and positive clones were identified by the presence of a 1-kb PCR product that is absent in Ax2 cells (Fig. 2 B). The disruption of *Ddnhe1* was further confirmed by the absence of a PCR product from an RT-PCR reaction designed to detect the transcript of *Dd*NHE1 in chemotactically competent cells (Fig. 2 A).

Development of *Ddnhe1*$^-$ cells was not impaired, as indicated by similar expression in Ax2 and *Ddnhe1*$^-$ cells of developmentally regulated genes. Northern blot analysis confirmed that 6-h-stage *Ddnhe1*$^-$ cells expressed the cAMP receptor cAR1 and the G protein α2 subunit Gα2 (Fig. 2 C), indicating that they retain the ability to sense the chemoattractant cAMP. Consistent with an established role for mammalian NHE1 in pH_i homeostasis, *Dd*NHE1 was necessary for steady-state pH_i and for increased pH_i in response to cAMP (Fig. 2 D). After 6-h starvation, Ax2 cells had a resting pH_i of 6.58 ± 0.05 (n = 7) that increased to 7.14 ± 0.02 by 90 s with 2 μM cAMP. By 6 min, the pH_i had returned to basal levels. In contrast, *Ddnhe1*$^-$ cells had a lower resting pH_i of 6.48 ± 0.06 (n = 7) that increased to only 6.86 ± 0.07 with cAMP. Hence, *Dd*NHE1 is a predominant, although not exclusive, determinant in the cAMP-induced increase in pH_i. Stable expression of *Dd*NHE1-HA in *Ddnhe1*$^-$ cells (*Ddnhe1*$^-$*/Dd*NHE1) restored resting pH_i to 6.63 ± 0.07 (n = 3). In response to cAMP, the pH_i of 7.29 ± 0.13 in *Ddnhe1*$^-$/DdNHE1 cells was higher and sustained for longer than in Ax2 cells, possibly because *Dd*NHE1, driven by the actin-15 promoter, was overexpressed.

Ddnhe1$^-$ cells lack polarity and have impaired chemotaxis

Although *Dd*NHE1 is not necessary for the expression of developmentally regulated genes, chemotaxis in response to cAMP was markedly impaired in all the *Ddnhe1*$^-$ clones generated. Using time-lapse video microscopy to visualize movement of individual cells toward a point source of cAMP delivered by a micropipette, Ax2 cells rapidly developed an elongated, polarized morphology with a defined front in the di-

rection of the point source of cAMP and pseudopodia that were restricted to the leading edge (Fig. 3, A and B; and Video 1, available at http://www.jcb.org/cgi/content/full/jcb.200412145/DC1). When the direction of the point source of cAMP was changed, Ax2 cells executed turns and retained the same leading and trailing edges characteristic of highly polarized cells (Fig. 3 C). In contrast, *Ddnhe1*$^-$ cells failed to adopt a polarized morphology in response to cAMP. They retained a rounded shape lacking a clear front and rear and extended pseudopodia around the entire cell (Fig. 3, A and B; and Video 2). In *Ddnhe1*$^-$*/Dd*NHE1 cells, a polarized morphology and leading edge pseudopodia were restored (Fig. 3, A and B; and Video 3, available at http://www.jcb.org/cgi/content/full/jcb.200412145/DC1).

Further analysis of time-lapse recordings indicated that the velocity of chemotaxing *Ddnhe1*$^-$ cells was decreased compared with Ax2 cells and *Ddnhe1*$^-$*/Dd*NHE1 cells (Fig. 4 A). Tracking of individual cells indicated that at 7 min most of the Ax2 and *Ddnhe1*$^-$*/Dd*NHE1 cells within the field showed directional movement toward cAMP. *Ddnhe1*$^-$ cells showed some movement, but it was random and not directed toward cAMP (Fig. 4 B, left). At 15 min, all Ax2 and *Ddnhe1*$^-$*/Dd*NHE1 cells within the field reached the point source of cAMP. *Ddnhe1*$^-$ cells eventually reached the point source but not until 30 min (Fig. 4 B, middle). At 30 min, however, *Ddnhe1*$^-$ cells were still not polarized, retaining mislocalized pseudopodia and failing to adopt an elongated morphology. *Ddnhe1*$^-$ cells lacked polarity, regardless of their distance from the chemoattractant source, as indicated by sequential traces of cells at distances of 15 and 45 μm from the micropipette delivering cAMP (Fig. 4 B, right).

F-actin localization and the kinetics of actin polymerization are impaired in *Ddnhe1*$^-$ cells

Consistent with impaired polarity, F-actin was mislocalized in *Ddnhe1*$^-$ cells and de novo actin polymerization was markedly attenuated. In polarized Ax2 cells chemotaxing toward a point source of cAMP, F-actin was predominantly at the leading edge and to a slight extent at the sides and the rear (Fig. 5 A). In contrast, F-actin in *Ddnhe1*$^-$ cells extended around the cell cortex and was not localized to the cell pole facing the point source of cAMP (Fig. 5 A). Similar to Ax2 cells, F-actin in *Ddnhe1*$^-$ cells was predominantly localized to areas where pseudopods were extending, although in *Ddnhe1*$^-$ cells pseudopodia were mislocalized and not confined to the direction of chemoattractant.

Because actin polymerization is a predominant driving force for pseudopod extension (Condeelis et al., 1990; Pollard and Borisy, 2003), mislocalized pseudopodia in *Ddnhe1*$^-$ cells suggested an inability to correctly regulate F-actin assembly. This prediction was confirmed by measuring time-dependent actin polymerization in response to cAMP. Total F-actin with a uniform concentration of 2 μM cAMP was determined in chemotactically competent cells in the presence of 5 mM caffeine to inhibit endogenous cAMP production. Ax2 cells had a characteristic biphasic increase in F-actin, as previously described (Condeelis et al., 1988; Chen et al., 2003; Park et al., 2004). The rapid first phase consisted of a 2.2-fold increase in F-actin that peaked between 4 to 8 s and returned to basal level by 16 s. A second, more sustained phase with a smaller amplitude peaked at 120 s after cAMP stimulation (Fig. 5 B). *Ddnhe1*$^-$ cells had similar levels of F-actin in the absence of cAMP compared with Ax2 cells and a biphasic increase in F-actin in response to cAMP. The magnitude of the first phase, however, was reduced by ~60% compared with Ax2 cells (Fig. 5 B). At 16 s, F-actin in *Ddnhe1*$^-$ cells returned to below basal level. The second phase was largely absent with an initial slight increase in F-actin that was not sustained after 30 s. In *Ddnhe1*$^-$*/Dd*NHE cells, the kinetics of actin polymerization was restored and the magnitude of the second phase was slightly increased compared with Ax2 cells (Fig. 5 B). Hence, *Dd*NHE1 does not regulate the abundance of F-actin in starved cells but is necessary for rapid F-actin assembly and for a leading edge localization of F-actin in response to cAMP. These data are consistent with findings in sea urchin

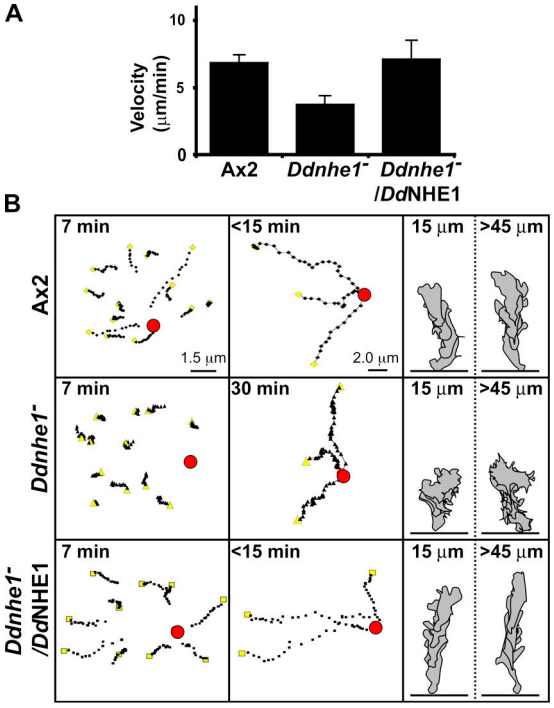

Figure 4. ***Ddnhe1*$^-$ cells chemotax toward cAMP but inefficiently and with decreased velocity.** (A) The velocity of Ax2 and *Ddnhe1*$^-$*/Dd*NHE1 cells was similar (7 and 8 μm/min, respectively), whereas the velocity of *Ddnhe1*$^-$ cells reduced by ~35% (4 μm/min). Data are expressed as the mean ± SEM of three independent cell preparations. (B) Tracking of individual cells for 7 min after addition of cAMP indicated that Ax2 cells (top left) and *Ddnhe1*$^-$*/Dd*NHE1 cells (bottom left), but not *Ddnhe1*$^-$ cells (middle left), had moved toward the point source of chemoattractant. Yellow squares and triangles mark the starting positions of tracked cells. After 15 min, all Ax2 cells (top) and *Ddnhe1*$^-$*/Dd*NHE1cells (bottom) within the field had reached the cAMP source, whereas *Ddnhe1*$^-$ cells took 30 min or more (middle). Four sequential traces taken from images obtained at 30-s intervals were obtained for chemotaxing Ax2 (top right), *Ddnhe1*$^-$ (middle right), and *Ddnhe1*$^-$*/Dd*NHE1 (bottom right) cells. The location of the needle containing cAMP was initially either within 15 μm or >45 μm, as indicated, from the leading edge of the cell.

eggs (Begg and Rebhun, 1979) and in mammalian fibroblasts (unpublished data), which suggest that increases in pH_i are not necessary for steady-state actin filament assembly but are required for "bursts" of de novo F-actin formation as a dynamic response to extracellular cues.

Ddnhe1⁻ cells have a sustained increase in membrane-associated $PI_{(3,4,5)}P_3$

cAMP induces a biphasic increase in the abundance of $PI_{(3,4,5)}P_3$ (Chen et al., 2003; Postma et al., 2003), correlating with the biphasic kinetics of actin polymerization. $PI_{(3,4,5)}P_3$ abundance was determined by using a reporter construct of a GFP-tagged pleckstrin homology (PH) domain of the cytosolic regulator of adenylyl cyclase (CRAC; GFP-PH^{CRAC}). The PH domain of CRAC binds $PI_{(3,4,5)}P_3$ and has been used to determine the localization and abundance of $PI_{(3,4,5)}P_3$ in chemotaxing *Dictyostelium* cells (Parent et al., 1998; Chen et al., 2003; Postma et al., 2003). With a uniform concentration of 2 μM cAMP, Ax2 and *Ddnhe1*⁻ cells both had biphasic increases in the abundance of membrane-associated (p100 fraction) GFP-PH^{CRAC} (Fig. 6 A); however, there were marked differences. Although the maximal abundance of GFP-PH^{CRAC} in the first phase was similar, in unstimulated *Ddnhe1*⁻ cells there was significantly more membrane-associated GFP-PH^{CRAC} and hence the fold increase was markedly less (1.2) compared with Ax2 cells (2.2). Additionally, although the kinetics of the second phase was similar, *Ddnhe1*⁻ cells had markedly more membrane-associated GFP-PH^{CRAC} at all time points.

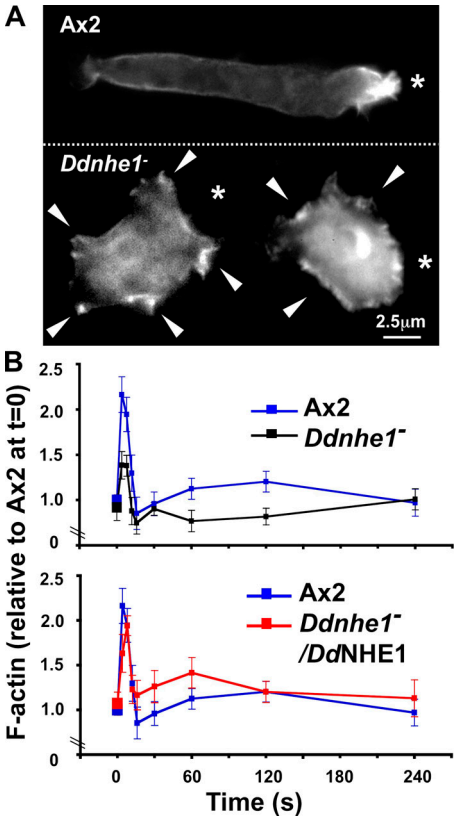

Figure 5. **Localization and production of F-actin in response to cAMP are impaired in chemotactically competent *Ddnhe1*⁻ cells.** (A) In Ax2 cells (top), F-actin was localized predominantly at the leading edge of the cell, and F-actin-rich protrusions were limited to the direction of the chemoattractant source (asterisks). In *Ddnhe1*⁻ cells (bottom), F-actin was distributed along the cell cortex, and although membrane protrusions (arrowheads) also contained F-actin, protrusions were not limited to the direction of the chemoattractant source but were seen around the cell. (B) Time course of F-actin production in response to a uniform concentration of 2 μM cAMP indicated a characteristic biphasic response in Ax2 cells (blue line), including a rapid (<10 s) first phase of greater magnitude and a slower and smaller second phase. In *Ddnhe1*⁻ cells (black line), the increase in F-actin in the first phase was reduced by ~60% and the second phase was transient with reduced F-actin formation, compared with Ax2 cells. *Ddnhe1*⁻*/Dd*NHE1 cells (red line) had a biphasic increase in F-actin, although the magnitude of first and second phases was slightly greater compared with Ax2 cells. Data are expressed as the mean ± SEM of at least three independent cell preparations.

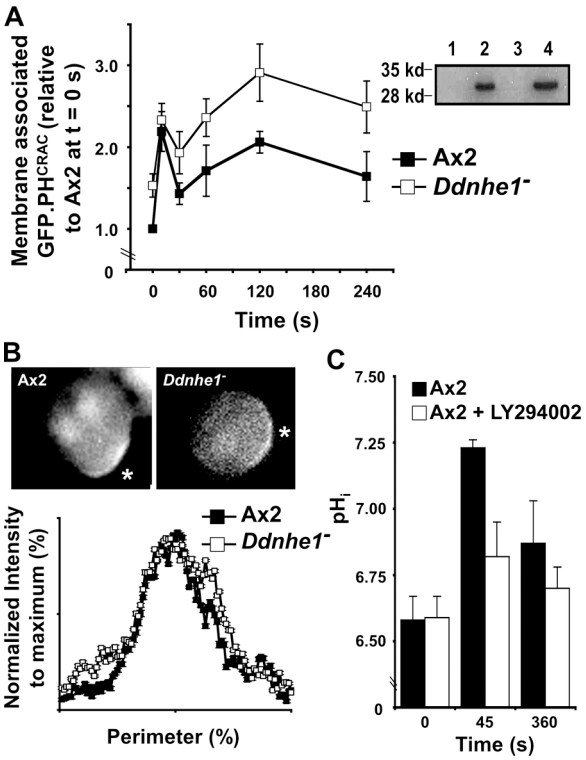

Figure 6. ***Ddnhe1*⁻ cells have increased abundance of membrane-associated PH^{CRAC}:GFP in the absence and presence of cAMP but retain directional sensing.** (A) Abundance of PH^{CRAC}:GFP in p100 membrane fractions and in total cell lysates was determined by immunoblotting with anti-GFP antibodies and used as a reporter for $PI_{(3,4,5)}P_3$ production. Ax2 cells and *Ddnhe1*⁻ cells had a biphasic increase in the abundance of membrane-associated PH^{CRAC}:GFP relative to total PH^{CRAC}:GFP in response to cAMP; however, in *Ddnhe1*⁻ cells there was more membrane-associated PH^{CRAC}:GFP in the absence of cAMP (time 0) and during the second phase compared with Ax2 cells. Data are expressed as the mean ± SEM of five independent experiments. (A, inset) Ax2 and *Ddnhe1*⁻ cells have similar expression of PH^{CRAC}:GFP, as indicated by immunoblotting with anti-GFP antibodies of total lysates of Ax2 cells untransformed (lane 1) and transformed with PH^{CRAC}:GFP (lane 2) and *Ddnhe1*⁻ cells untransformed (lane 3) and transformed with PH^{CRAC}:GFP (lane 4). (B) Asymmetric translocation of cytosolic PH^{CRAC}:GFP to the membrane in latrunculin-treated cells indicates Ax2 and *Ddnhe1*⁻ sense and respond to a point source of 10 μM cAMP. Intensity of GFP fluorescence at the cortex was expressed by plotting intensity as a function of the percentage of the cell perimeter. Data represent the mean ± SEM of values obtained for cells in two separate preparations. (C) The cAMP-induced increase in pH_i of Ax2 cells was attenuated by the presence of Ly294002. Data represent the mean ± SEM of four independent determinations.

Ddnhe1⁻ cells retain directional sensing

Ddnhe1⁻ cells express the developmentally regulated genes cAR1 and Gα2 and chemotax toward cAMP, albeit inefficiently, which suggests they retain directional sensing. This finding was confirmed by the ability of *Ddnhe1⁻* cells to asymmetrically accumulate $PI_{(3,4,5)}P_3$ in the direction of a point source of cAMP. Directional sensing, which does not require polarity or rapid actin filament assembly (Devreotes and Janetopoulos, 2003), was determined in cells treated with latrunculin A to inhibit actin polymerization. Although latrunculin-treated cells were round and lacked morphological polarity, in Ax2 and *Ddnhe1⁻* cells GFP-PH^{CRAC} was predominantly localized in an arc along the plasma membrane closest to the pipette delivering cAMP (Fig. 6 B). An analysis of GFP-PH^{CRAC} intensity as a function of cell perimeter revealed nearly superimposable tracings for Ax2 and *Ddnhe1⁻* cells. Collectively, therefore, our data indicate that *Dd*NHE1 is not necessary for cells to detect an asymmetric extracellular cue but is essential for establishing morphological polarity and efficient chemotaxis toward the cue.

The ability of *Ddnhe1⁻* cells to acquire asymmetric localization of GFP-PH^{CRAC} suggested *Dd*NHE1 might act downstream of $PI_{(3,4,5)}P_3$ production by phosphatidylinositol 3 (PI3)–kinases. This prediction was tested by determining cAMP-induced increases in pH_i in the absence and presence of LY294002, which inhibits PI3-kinase activity. In Ax2 cells treated with 30 μM LY294002, the increase in pH_i with cAMP was markedly attenuated (Fig. 6 C). In *Ddnhe1⁻* cells, the pH_i response to cAMP was similar in the absence and presence of LY294002 (unpublished data). Hence, inhibition of PI3-kinase blocks *Dd*NHE1-dependent, but not *Dd*NHE1-independent, increases pH_i in response to cAMP.

Discussion

In differentiated *Dictyostelium* cells, cAMP induces an increase in pH_i (Jamieson et al., 1984; Aerts et al., 1987) that is essential for directional movement (Van Duijn and Inouye, 1991). However, the ion transport process regulating pH_i homeostasis and the mechanism whereby pH_i regulates chemotaxis in *Dictyostelium* cells have not been clearly defined. We now report that a *Dictyostelium* Na-H exchanger, *Dd*NHE1, is the predominant regulator of increased pH_i in response to cAMP and is necessary for efficient chemotaxis. Although *Ddnhe1⁻* cells retain directional sensing, they lack morphological polarity, have decreased de novo actin polymerization, and fail to localize F-actin at the leading edge, resulting in impaired chemotaxis.

A rapid increase in actin filament assembly is the major driving force for directed cell motility (Condeelis et al., 1990; Pollard and Borisy, 2003). In response to chemoattractant, *Dictyostelium* cells have a biphasic increase in actin filament assembly (Chen et al., 2003; Park et al., 2004). In *Ddnhe1⁻* cells, the rapid (<10 s) first phase is markedly attenuated and the prolonged (30 to 180 s) second phase is largely absent. The first phase of actin polymerization may be essential for establishing morphological asymmetry, and *Ddnhe1⁻* cells never develop polarity, regardless of their distance from the chemoattractant source. Where actin polymerization is sustained determines the direction of cell movement, and *Dd*NHE1, which localizes predominantly at the front of polarized cells, is also necessary for limiting F-actin assembly to the leading edge.

Several models have recently been proposed for how the first and second phases of actin polymerization are controlled (Chen et al., 2003; Mouneimne et al., 2004; Park et al., 2004; Sasaki et al., 2004). All models predict that the first phase is independent of $PI_{(3,4,5)}P_3$, and, consistent with this prediction, in *Ddnhe1⁻* cells when the first phase of actin polymerization is suppressed the abundance of membrane-associated $PI_{(3,4,5)}P_3$ is normal. In *Dictyostelium* cells, the first phase of actin polymerization is in part dependent on Rac1B (Park et al., 2004) and Ras proteins (Sasaki et al., 2004). *Dictyostelium* cells null for *RacB* have an actin polymerization profile similar to that of *Ddnhe1⁻* cells, including ∼60% decrease in the magnitude of the first phase and a markedly suppressed second phase (Park et al., 2004). In *RacB*-null cells, but not in *Ddnhe1⁻* cells, however, the basal abundance of F-actin is reduced compared with wild-type cells. Another distinction is that *RacB*-null cells exhibit only a small loss of polarity compared with the marked lack of polarity in *Ddnhe1⁻* cells. *Dictyostelium* Ras proteins also regulate the first phase of actin polymerization and polarity. Although *Dictyostelium* cells null for *RasG* have normal polarity and only slightly reduced F-actin in response to cAMP, expression of a dominant inactive *Dd*RasG-S17N in *RasG*-null mutants to block activation of other Ras proteins results in loss of polarity and ∼30% reduction in the initial F-actin peak (Sasaki et al., 2004). The role of *Dd*NHE1 in chemotaxis may be distinct from that of RacB or Ras because the phenotype of *Ddnhe1⁻* cells is similar to *RacB*-null cells in F-actin formation, but not in morphological polarity, and similar to *RasG*-null cells expressing *Dd*RasG-S17N in loss of polarity, but not in the regulation of actin polymerization.

In mammalian cells, the first phase of actin polymerization is preceded by an increase in actin free barbed ends generated by the actin-severing protein cofilin (Mouneimne et al., 2004). Because the actin-severing activity of cofilin is pH-sensitive, cofilin is a possible candidate mediating pH-dependent effects of *Dd*NHE1 on the first phase of actin filament assembly. Increased pH_i is necessary to stimulate cofilin activity and to promote the recruitment of cofilin to the leading edge membrane of migrating cells (Bernstein et al., 2000; Bowman et al., 2000). In addition to cofilin, possible targets of *Dd*NHE1-dependent increases in pH_i include severin, an actin-severing and -capping protein of the pH-sensitive gelsolin family (Yin et al., 1990; Lamb et al., 1993), and hisactophilin, a pH sensor in *Dictyostelium* that nucleates actin filaments (Hanakam et al., 1996; Stoeckelhuber et al., 1996).

The second phase of actin polymerization is dependent on the abundance and localization of $PI_{(3,4,5)}P_3$, which are regulated by PI3-kinases and the PI3-phosphatase PTEN (Funamoto et al., 2002; Iijima and Devreotes, 2002). In *pi3k1⁻/2⁻* cells and in cells treated with pharmacological inhibitors of PI3-kinases, the second phase of actin polymerization is suppressed but the first phase is retained (Funamoto et al., 2001;

Chen et al., 2003). Consistent with previous papers that showed mammalian NHE1 may act downstream of PI3-kinases (Ma et al., 1994; Reshkin et al., 2000), the PI3-kinase inhibitor LY294002 completely blocks the *Dd*NHE1-dependent increase in pH_i in response to cAMP. Two predictions may explain why the second phase of actin polymerization is suppressed in *Ddnhe1*$^-$ cells despite increased $PI_{(3,4,5)}P_3$. *Dd*NHE1 could act downstream of $PI_{(3,4,5)}P_3$ in a pathway regulating the second phase of actin polymerization, but, in contrast to a positive feedback loop suggested between actin polymerization and $PI_{(3,4,5)}P_3$ (Weiner et al., 2002; Srinivasan et al., 2003; Sasaki et al., 2004), increased pH_i may act in a negative feedback mechanism to limit $PI_{(3,4,5)}P_3$ abundance. Alternatively, *Dd*NHE1 regulates the second phase of actin polymerization independently of $PI_{(3,4,5)}P_3$.

Increased pH_i is predicted to be an evolutionarily conserved mechanism necessary for cytoskeletal filament assembly and for motility (Tilney et al., 1978; Begg and Rebhun, 1979; Italiano et al., 1999). Protons do not directly regulate filament assembly (Tilney et al., 1978; Begg and Rebhun, 1979; Italiano et al., 1999) but likely act on pH-dependent filament-binding proteins, such as cofilin and gelsolin. In *Dictyostelium* cells, a pH-dependent increase in actin polymerization may be a developmentally regulated mechanism to control polarity because *Dd*NHE1 is expressed in chemotactically competent cells but not in vegetative cells. In neutrophil-like HL60 cells, which are chemotactic only after differentiation, NHE1 is expressed in differentiated, but not in undifferentiated, cells (unpublished data). In fibroblasts (Denker and Barber, 2002) and epithelial cells (Klein et al., 2000), NHE1 also is necessary for directional migration but its expression at the plasma membrane is constitutive.

However, whether *Dd*NHE1 regulates chemotaxis exclusively through increased H^+ efflux or also by undetermined pH-independent actions remains to be determined. Independently of generating H^+ efflux, mammalian NHE1 also anchors actin filaments by binding ERM (ezrin, moesin, and radixin) actin-binding proteins. Actin anchoring by NHE1, but not H^+ efflux, is necessary for the bundling of actin stress fibers, localizing NHE1, and tethering actin filaments in specialized membrane domains (Denker and Barber, 2002). Although ERM proteins have not been identified in *Dictyostelium*, a GST-fusion protein containing the NH_2-terminal FERM (protein 4.1 and ERM) domain of moesin binds directly to *Dd*NHE1 (unpublished data), suggesting that binding of a FERM domain–containing protein might maintain *Dd*NHE1 at the cell front. We predict that the localization of NHE1 and *Dd*NHE1 at the front of motile cells retains a leading edge H^+ efflux that is necessary for cell polarity and directional movement.

Materials and methods

Cell culture and starvation

Cells were grown in Knecht medium under standard conditions (Sussman, 1987), and exponentially growing cells were harvested for use in all experiments. Chemotactic competence was induced by starving cells for 6 h in phosphate buffer (PB; 20 mM KH_2PO_4, and 20 mM K_2HPO_4, pH 6.8) at RT at a cell density of 1×10^7 to 2×10^7 cells/ml while shaking at 115 rpm.

Isolation of *Dd*NHE1 and the generation of *Ddnhe1*$^-$ cells

Total RNA was isolated (QIAGEN; UC-100) from wild-type Ax2 cells (provided by C.J. Weijer, University of Dundee, Dundee, Scotland, UK), and RT-PCR was performed on chemotactically competent cells using primers designed to the NH_2 and COOH termini of *Dd*NHE1 (AA052201) (5′GGATCCATGAAATTGAACAAAAGTTATATATTAATAGTTG-3′ and 5′GGGCCCTTAGTATGGGTAGTCGACTGGGTCGTAAGCACATCATTG-GAGTGATGTTGGCTGTTATTG-3′, respectively). The COOH terminus primer also contained an HA-epitope tag (underlined), and both primers contained restriction sites (NH_2 terminus, BamHI; COOH terminus, SmaI) for cloning. The single PCR product obtained was cloned into the TOPO2.1 cloning vector and subcloned into pB17S, a *Dictyostelium* expression vector containing a neomycin resistance-conferring cassette, which was used in reconstituting *Dd*NHE1-HA into *Ddnhe1*$^-$ cells.

To generate *Ddnhe*$^-$ cells, Ax2 cells were electroporated (Howard et al., 1988) with ~0.1 μg of linearized DNA consisting of a blasticidin resistance cassette (Bst^r) excised from the *Dictyostelium* expression vector pUC118 (provided by C.J. Weijer) flanked by regions of *Dd*NHE1. Three different constructs were used for three independent transformations, and individual clones were isolated from each transformation after selection with 10 μg/ml of Blasticidin. Two of the constructs consisted of the Bst^r cassette inserted into partial *Dd*NHE1 PCR products of two lengths (1 and 1.5 kb), and the third construct consisted of the Bst^r cassette inserted into the 1.5-kb PCR product after excision of ~200 bp of *Dd*NHE1. Positive clones were identified by the absence of the *Dd*NHE1 transcript from chemotactically competent cells (Fig. 2 A) and by the presence of a PCR product from genomic DNA by using a primer set consisting of one within the Bst^r cassette and another within the genomic region near *Dd*NHE1 (Fig. 2 B).

Surface biotinylation

Starved *Ddnhe1*$^-$/*Dd*NHE1-HA cells and Ax2 cells expressing the PH domain of CRAC fused to GFP (PH^{CRAC}:GFP; provided by P. Devreotes, Johns Hopkins University, Baltimore, MD) were labeled for 30 min on ice with 0.5 mg/ml of biotin in KK_2 buffer (EZ-Link Sulfo-NHS-LC-Biotin; Pierce Chemical Co.). Cells were washed in ice-cold KK_2 buffer three times and lysed with RIPA buffer (50 mM Tris-HCl, 150 mM NaCl, 1 mM EDTA, 1% NP-40, 0.5% deoxycholate, 0.1% SDS, and protease inhibitors, pH 7.5). Samples were cleared with protein G–Sepharose (17–0618-01; Amersham Biosciences) at 4°C. Supernatant was collected and incubated with anti-HA (1:250, 12CA5; Roche), anti-cAR1 (1:250; provided by C. Parent, National Cancer Institute, Bethesda, MD), or anti-GFP (1:250, J108; CLONTECH Laboratories, Inc.) antibodies in the presence of protein G–Sepharose at 4°C. Sepharose beads were washed three times in ice-cold RIPA Buffer, resuspended in loading buffer, and heated to 100°C for 5 min. Samples were subjected to 10% SDS-PAGE and transferred onto polyvinylidene difluoride membranes. Membranes were blocked with 5% milk and probed with HRP/Streptavidin (1:1000; Vector Laboratories). Data are representative of three independent cell preparations.

Northern blot analysis

Total RNA was isolated from Ax2 and *Ddnhe1*$^-$ cells before starvation and after 3 and 6 h of starvation in PB. 4 μg of total RNA was separated using gel electroporesis, transferred to nylon membranes (Hybond-N+; Amersham Biosciences), and probed with ^{32}P-labeled cAR1 or Gα2 DNA probes. The membranes were stripped and reprobed for the ribosomal protein IG7 (provided by P. Schaap, University of Dundee) for loading control. Data are representative of Northern blots of two separate RNA preparations.

pH_i measurements

pH_i was determined in cells loaded with the pH-sensitive fluorescent dye 2′,7′-bis-(2-carboxyethyl) 5- (and -6)-carboxyfluorescein (BCECF; Molecular Probes). During starvation of cells for 6 h, 5 μM BCECF was added for the final 30 min, 5 mM caffeine was added for the last 20 min, cells were washed once in PB, resuspended in PB containing 5 mM caffeine, and 5×10^5 cells were added to wells of a 96-well plate. Cells were allowed to attach for 5 min before removing excess cells and submerging the attached cells in 40 μl PB, pH 6.8, containing 5 mM caffeine. In parallel wells, 40 μl PB at pH 5.9, 6.8, and 7.0 containing 5 μM nigericin (Molecular Probes) was added to equalize intracellular and extracellular pH and calibrate fluorescence intensity to pH_i. After 15 min, the fluorescence intensity was determined by using a SpectraMax Gemini XS Micro Plate fluorometer (Molecular Devices) at excitation wavelengths of 439 nm (H^+-insensitive) and 490 nm (H^+-sensitive) with an emission wavelength of 530 nm. A plot of the 490/439 nm ratios against the pH values of the

buffers containing nigericin was used to generate a calibration curve from which pH_i was determined. To determine pH_i in response to cAMP, 2 μM was added to cells and the fluorescence intensity was determined at 45-s intervals. After 6 min, the fluorescence intensity at 439 and 490 nm was determined to confirm that fluorescence intensity at 439 remained constant. Determinations were performed in triplicate, and data were expressed as the mean ± SEM of the indicated independent cell preparations. Inhibition of PI3-kinases was achieved by incubating cells with 30 μM Ly294002 during the caffeine treatment.

Chemotaxis assays and cell tracking

For the analysis of individual cell movement, chemotactically competent cells were basalized for 20 min by adding 5 mM caffeine and then plated at a density of $\sim 10^3$ cells/cm^2 on nonnutrient 1% phosphate agar plates containing 5 mM caffeine. A micropipette containing 10 μM cAMP was placed next to cells, and images were captured every 30 s using a Spot LCD camera mounted on a microscope (model Axiovert S-100; Carl Zeiss MicroImaging, Inc.) with a 40× Hoffmann modulation objective and operated using Openlab software (Improvision). Cells were tracked using Openlab software, and their coordinates were plotted using Microsoft Excel software.

Phalloidin staining and immunolabeling of *Dd*NHE1

Cells were submerged in PB, allowed to develop on plastic dishes for 8 h, and washed and fixed for 3 min in PB containing 3.7% glutaraldehyde/0.1% Triton X-100. The fixative was removed, and the cells were washed three times in PB. To visualize F-actin, cells were incubated in PB containing rhodamine phalloidin (Molecular Probes) for 1 h at RT. Cells were washed three times in PB and dried briefly, and a drop of Vectashield was added before a glass coverslip was placed over the cells.

For immunolabeling of *Dd*NHE1, *Ddnhe*$^-$/*Dd*NHE1-HA cells were fixed and washed as described in the previous paragraph, followed by blocking in PB containing 5% FBS for 30 min at RT. Cells were labeled for 1 h at RT with anti-HA antibodies (12CA5; Roche) at a dilution of 1:500 in PB containing 2% FBS. Cells were washed three times in PB and incubated at RT in PB containing FITC labeled anti–mouse IgG (Jackson ImmunoResearch Laboratories) for 1 h. Cells were washed three times in PB and allowed to dry briefly, and a drop of Vectashield was added before a glass coverslip was placed over the cells. Images were captured using an inverted confocal microscope (model LSM500; Carl Zeiss MicroImaging, Inc.) and three-dimensional projection images were generated using LSM software.

Actin polymerization assays

Starved cells basalized with 5 mM caffeine at a density of 2×10^7 cells/ml were stimulated with a uniform concentration of 2 μM cAMP for the indicated times and F-actin was determined as previously described (Steimle et al., 2001). Reactions were stopped by adding fixing buffer (100 mM MES, 5 mM EDTA, 10 mM $MgCl_2$, and 1% Triton X-100, pH 6.8) and incubating for 15 min at RT. Samples were centrifuged for 5 min at 14,000 rpm, the supernatant removed, and cell pellets resuspended in sample loading buffer and boiled for 10 min. Samples were separated by 12% SDS-PAGE, proteins stained with Coomassie blue, and the predominant band, which was actin, quantified by using National Institutes of Health (NIH) image analysis software. Results were expressed as the mean ± SEM of three or more independent experiments.

Membrane-associated PH^{CRAC}:GFP

Ax2 cells and *Ddnhe1*$^-$ cells were transformed with the reporter construct PH^{CRAC}:GFP, which binds $PI_{(3,4,5)}P_3$. Chemotactically competent cells were basalized in 5 mM caffeine and washed two times in PB before stimulation with 2 μM cAMP for the indicated times. Ice-cold buffer (EDTA and Tris HCl, pH 8.0) was added and the cells were sonicated three times for 5 s each time. A postnuclear supernatant fraction was collected (total fraction) and centrifuged at 100,000 *g* for 20 min at 4°C to obtain particulate (p100) and soluble (s100) fractions. Samples were separated by 10% SDS-PAGE, transferred onto polyvinylidene difluoride membranes, blocked with 5% milk, and probed with anti-GFP monoclonal mouse antibodies (J108; CLONTECH Laboratories, Inc.). Intensity of the bands was determined by using NIH image analysis software, and results were expressed as the mean ± SEM of five independent experiments.

Directional sensing was determined in cells expressing PH^{CRAC}:GFP and starved for 6 h. Cells were treated with 5 mM caffeine and latrunculin (1 μM) for 20 min and plated onto nonnutrient 1% agar plates containing latrunculin and caffeine. Fluorescence images were acquired before (−5 s) and after (+5 s) placing a needle containing 10 μM cAMP at a distance of ~20 μm from the cell. Intensity of GFP fluorescence at the perimeter was determined using NIH image software, normalized to maximal fluorescence, and expressed as previously described (Janetopoulos et al., 2004) by plotting intensity as a function of the percent of the perimeter. Data represent the mean ± SEM of four cells from two independent cell preparations.

Online supplemental material

Time-lapse video microscopy (Fig. 3) of 6 h starved cells (Ax2, *Ddnhe1*$^-$, and *Ddnhe1*$^-$/DdNHE1) chemotaxing toward a pipette tip containing 10 μM cAMP is shown in Videos 1, 2, and 3, respectively. Images were captured at 30-s time intervals using a Spot LCD camera mounted on a microscope (Axiovert S-100; Carl Zeiss MicroImaging, Inc.) with a 40× Hoffmann modulation objective and operated using Openlab software (Improvision). Captured images were compiled into a QuickTime movie using Sorenson Video Compressor software. Online supplemental material is available at http://www.jcb.org/cgi/content/full/jcb.200412145/DC1.

We thank Henry Bourne, Marcel Meima, and Christian Frantz for comments and suggestions and Mary McKenney for editing the manuscript. We thank Kees Weijer, Peter Devreotes, Carole Parent, and Pauline Schaap for providing reagents.

This work was supported by National Institutes of Health grant GM58642 and an award from the Sandler Program in Basic Sciences. This investigation was conducted in a facility constructed with support from Research Facilities Improvement Program grant C06 RR16490 from the National Center for Research Resources, National Institutes of Health.

Submitted: 22 December 2004
Accepted: 10 March 2005

References

Aerts, R.J., R.J. De Wit, and M.M. Van Lookeren Campagne. 1987. Cyclic AMP induces a transient alkalinization in *Dictyostelium*. *FEBS Lett.* 220: 366–370.

Begg, D.A., and L.I. Rebhun. 1979. pH regulates the polymerization of actin in the sea urchin egg cortex. *J. Cell Biol.* 83:241–248.

Bernstein, B.W., W.B. Painter, H. Chen, L.S. Minamide, H. Abe, and J.R. Bamburg. 2000. Intracellular pH modulation of ADF/cofilin proteins. *Cell Motil. Cytoskeleton.* 47:319–336.

Bowman, G.D., I.M. Nodelman, Y. Hong, N.H. Chua, U. Lindberg, and C.E. Schutt. 2000. A comparative structural analysis of the ADF/cofilin family. *Proteins.* 41:374–384.

Chen, L., C. Janetopoulos, Y.E. Huang, M. Iijima, J. Borleis, and P.N. Devreotes. 2003. Two phases of actin polymerization display different dependencies on PI(3,4,5)P3 accumulation and have unique roles during chemotaxis. *Mol. Biol. Cell.* 14:5028–5037.

Condeelis, J., A. Hall, A. Bresnick, V. Warren, R. Hock, H. Bennett, and S. Ogihara. 1988. Actin polymerization and pseudopod extension during amoeboid chemotaxis. *Cell Motil. Cytoskeleton.* 10:77–90.

Condeelis, J., A. Bresnick, M. Demma, S. Dharmawardhane, R. Eddy, A.L. Hall, R. Sauterer, and V. Warren. 1990. Mechanisms of amoeboid chemotaxis: an evaluation of the cortical expansion model. *Dev. Genet.* 11: 333–340.

Denker, S.P., and D.L. Barber. 2002. Cell migration requires both ion translocation and cytoskeletal anchoring by the Na-H exchanger NHE1. *J. Cell Biol.* 159:1087–1096.

Denker, S.P., D.C. Huang, J. Orlowski, H. Furthmayr, and D.L. Barber. 2000. Direct binding of the Na–H exchanger NHE1 to ERM proteins regulates the cortical cytoskeleton and cell shape independently of H^+ translocation. *Mol. Cell.* 6:1425–1436.

Devreotes, P., and C. Janetopoulos. 2003. Eukaryotic chemotaxis: distinctions between directional sensing and polarization. *J. Biol. Chem.* 278:20445–20448.

Etienne-Manneville, S., and A. Hall. 2002. Rho GTPases in cell biology. *Nature.* 420:629–635.

Funamoto, S., K. Milan, R. Meili, and R.A. Firtel. 2001. Role of phosphatidylinositol 3′ kinase and a downstream pleckstrin homology domain–containing protein in controlling chemotaxis in *Dictyostelium*. *J. Cell Biol.* 153:795–810.

Funamoto, S., R. Meili, S. Lee, L. Parry, and R.A. Firtel. 2002. Spatial and temporal regulation of 3-phosphoinositides by PI 3-kinase and PTEN mediates chemotaxis. *Cell.* 109:611–623.

Goyal, S., G. Vanden Heuvel, and P.S. Aronson. 2003. Renal expression of novel Na^+/H^+ exchanger isoform NHE8. *Am. J. Physiol. Renal Physiol.* 284:F467–F473.

Hanakam, F., G. Gerisch, S. Lotz, T. Alt, and A. Seelig. 1996. Binding of hisactophilin I and II to lipid membranes is controlled by a pH-dependent myristoyl-histidine switch. *Biochemistry.* 35:11036–11044.

Howard, P.K., K.G. Ahern, and R.A. Firtel. 1988. Establishment of a transient expression system for *Dictyostelium discoideum*. *Nucleic Acids Res.* 16: 2613–2623.

Iijima, M., and P. Devreotes. 2002. Tumor suppressor PTEN mediates sensing of chemoattractant gradients. *Cell.* 109:599–610.

Italiano, J.E., Jr., M. Stewart, and T.M. Roberts. 1999. Localized depolymerization of the major sperm protein cytoskeleton correlates with the forward movement of the cell body in the amoeboid movement of nematode sperm. *J. Cell Biol.* 146:1087–1096.

Jamieson, G.A., Jr., W.A. Frazier, and P.H. Schlesinger. 1984. Transient increase in intracellular pH during *Dictyostelium* differentiation. *J. Cell Biol.* 99:1883–1887.

Janetopoulos, C., L. Ma, P.N. Devreotes, and P.A. Iglesias. 2004. Chemoattractant-induced phosphatidylinositol 3,4,5-trisphosphate accumulation is spatially amplified and adapts, independent of the actin cytoskeleton. *Proc. Natl. Acad. Sci. USA.* 101:8951–8956.

King, K.L., J. Essig, T.M. Roberts, and T.S. Moerland. 1994. Regulation of the *Ascaris* major sperm protein (MSP) cytoskeleton by intracellular pH. *Cell Motil. Cytoskeleton.* 27:193–205.

Klein, M., P. Seeger, B. Schuricht, S.L. Alper, and A. Schwab. 2000. Polarization of Na^+/H^+ and Cl^-/HCO_3^- exchangers in migrating renal epithelial cells. *J. Gen. Physiol.* 115:599–608.

Lamb, J.A., P.G. Allen, B.Y. Tuan, and P.A. Janmey. 1993. Modulation of gelsolin function. Activation at low pH overrides Ca^{2+} requirement. *J. Biol. Chem.* 268:8999–9004.

Ma, Y.H., H.P. Reusch, E. Wilson, J.A. Escobedo, W.J. Fantl, L.T. Williams, and H.E. Ives. 1994. Activation of Na^+/H^+ exchange by platelet-derived growth factor involves phosphatidylinositol 3′-kinase and phospholipase C gamma. *J. Biol. Chem.* 269:30734–30739.

Mouneimne, G., L. Soon, V. DesMarais, M. Sidani, X. Song, S.C. Yip, M. Ghosh, R. Eddy, J.M. Backer, and J. Condeelis. 2004. Phospholipase C and cofilin are required for carcinoma cell directionality in response to EGF stimulation. *J. Cell Biol.* 166:697–708.

Nelson, W.J. 2003. Adaptation of core mechanisms to generate cell polarity. *Nature.* 422:766–774.

Parent, C.A. 2004. Making all the right moves: chemotaxis in neutrophils and *Dictyostelium*. *Curr. Opin. Cell Biol.* 16:4–13.

Parent, C.A., B.J. Blacklock, W.M. Froehlich, D.B. Murphy, and P.N. Devreotes. 1998. G protein signaling events are activated at the leading edge of chemotactic cells. *Cell.* 95:81–91.

Park, K.C., F. Rivero, R. Meili, S. Lee, F. Apone, and R.A. Firtel. 2004. Rac regulation of chemotaxis and morphogenesis in *Dictyostelium*. *EMBO J.* 23:4177–4189.

Pollard, T.D., and G.G. Borisy. 2003. Cellular motility driven by assembly and disassembly of actin filaments. *Cell.* 112:453–465.

Postma, M., J. Roelofs, J. Goedhart, T.W. Gadella, A.J. Visser, and P.J. Van Haastert. 2003. Uniform cAMP stimulation of *Dictyostelium* cells induces localized patches of signal transduction and pseudopodia. *Mol. Biol. Cell.* 14:5019–5027.

Reshkin, S.J., A. Bellizzi, V. Albarani, L. Guerra, M. Tommasino, A. Paradiso, and V. Casavola. 2000. Phosphoinositide 3-kinase is involved in the tumor-specific activation of human breast cancer cell Na^+/H^+ exchange, motility, and invasion induced by serum deprivation. *J. Biol. Chem.* 275: 5361–5369.

Sasaki, A.T., C. Chun, K. Takeda, and R.A. Firtel. 2004. Localized Ras signaling at the leading edge regulates PI3K, cell polarity, and directional cell movement. *J. Cell Biol.* 167:505–518.

Srinivasan, S., F. Wang, S. Glavas, A. Ott, F. Hofmann, K. Aktories, D. Kalman, and H.R. Bourne. 2003. Rac and Cdc42 play distinct roles in regulating $PI(3,4,5)P_3$ and polarity during neutrophil chemotaxis. *J. Cell Biol.* 160:375–385.

Steimle, P.A., S. Yumura, G.P. Cote, Q.G. Medley, M.V. Polyakov, B. Leppert, and T.T. Egelhoff. 2001. Recruitment of a myosin heavy chain kinase to actin-rich protrusions in *Dictyostelium*. *Curr. Biol.* 11:708–713.

Stoeckelhuber, M., A.A. Noegel, C. Eckerskorn, J. Kohler, D. Rieger, and M. Schleicher. 1996. Structure/function studies on the pH-dependent actin-binding protein hisactophilin in *Dictyostelium* mutants. *J. Cell Sci.* 109: 1825–1835.

Sussman, M. 1987. Cultivation and synchronous morphogenesis of *Dictyostelium* under controlled experimental conditions. *Methods Cell Biol.* 28:9–29.

Tilney, L.G., D.P. Kiehart, C. Sardet, and M. Tilney. 1978. Polymerization of actin. IV. Role of Ca++ and H+ in the assembly of actin and in membrane fusion in the acrosomal reaction of echinoderm sperm. *J. Cell Biol.* 77:536–550.

Van Duijn, B., and K. Inouye. 1991. Regulation of movement speed by intracellular pH during *Dictyostelium discoideum* chemotaxis. *Proc. Natl. Acad. Sci. USA.* 88:4951–4955.

Wang, D., S.M. King, T.A. Quill, L.K. Doolittle, and D.L. Garbers. 2003. A new sperm-specific Na^+/H^+ exchanger required for sperm motility and fertility. *Nat. Cell Biol.* 5:1117–1122.

Weiner, O.D., P.O. Neilsen, G.D. Prestwich, M.W. Kirschner, L.C. Cantley, and H.R. Bourne. 2002. A $PtdInsP_3$- and Rho GTPase-mediated positive feedback loop regulates neutrophil polarity. *Nat. Cell Biol.* 4:509–513.

Yin, H.L., P.A. Janmey, and M. Schleicher. 1990. Severin is a gelsolin prototype. *FEBS Lett.* 264:78–80.